

# Nonequilibrium quasistationary spin disordered state in the Kitaev-Heisenberg magnet $\alpha$ -RuCl<sub>3</sub>

R. B. Versteeg,<sup>1,\*</sup> A. Chiochetta,<sup>2</sup> F. Sekiguchi,<sup>1</sup> A. I. R. Aldea,<sup>1</sup> A. Sahasrabudhe,<sup>1</sup> K. Budzinauskas,<sup>1</sup> Zhe Wang,<sup>1</sup> V. Tsurkan,<sup>3,4</sup> A. Loidl,<sup>4</sup> D. I. Khomskii,<sup>1</sup> S. Diehl,<sup>2</sup> and P. H. M. van Loosdrecht<sup>1,†</sup>

<sup>1</sup>*Institute of Physics II, University of Cologne, D-50937 Cologne, Germany*

<sup>2</sup>*Institute for Theoretical Physics, University of Cologne, D-50937 Cologne, Germany*

<sup>3</sup>*Institute of Applied Physics, MD 2028, Chisinau, Republic of Moldova*

<sup>4</sup>*Experimental Physics V, Center for Electronic Correlations and Magnetism, University of Augsburg, 86159 Augsburg, Germany*

(Dated: February 1, 2022)

Excitation by light pulses enables the manipulation of phases of quantum condensed matter. Here, we photoexcite high-energy holon-doublon pairs as a way to alter the magnetic free energy landscape of the Kitaev-Heisenberg magnet  $\alpha$ -RuCl<sub>3</sub>, with the aim to dynamically stabilize a proximate spin liquid phase. The holon-doublon pair recombination through multimagnon emission is tracked through the time-evolution of the magnetic linear dichroism originating from the competing zigzag spin ordered ground state. A small holon-doublon density suffices to reach a spin disordered state. The phase transition is described within a dynamic Ginzburg-Landau framework, corroborating the quasistationary nature of the transient spin disordered phase. Our work provides insight into the coupling between the electronic and magnetic degrees of freedom in  $\alpha$ -RuCl<sub>3</sub> and suggests a new route to reach a proximate spin liquid phase in Kitaev-Heisenberg magnets.

## INTRODUCTION

Light can be utilized as a tool to manipulate and engineer novel phases in quantum materials<sup>1</sup>. In particular, excitation via intense light pulses has been used to create nonequilibrium states of matter nonexistent at thermal equilibrium, such as transient superconductivity in underdoped cuprates<sup>2</sup>, metastable ferroelectricity in SrTiO<sub>3</sub><sup>3,4</sup>, and unconventional charge-density wave order in LaTe<sub>3</sub><sup>5</sup>. The light pulses excite a transient population of quasiparticles or collective excitations, which acts as a dynamic parameter to alter the material's free-energy landscape. For sufficiently strong excitation densities, a nonequilibrium phase transition can eventually occur<sup>5-7</sup>. By the same token, intense pulsed light holds promise to manipulate the spin state of frustrated magnets<sup>8,9</sup>. These materials, in fact, can host exotic and elusive phases, such as spin liquids (SL). Whereas SLs harbor rich many-body phenomena resulting from spin frustration and possible spin fractionalization<sup>10,11</sup>, these phases often compete with a magnetically ordered ground state, which is typically energetically favoured. Pulsed light excitation can then provide a mechanism to tip the energetic balance away from the magnetically ordered ground state towards a nonequilibrium proximate spin liquid phase.

We explore this concept for the Kitaev-Heisenberg frustrated magnet, a type of Mott insulator with a layered honeycomb structure and strong spin-orbit coupling<sup>12-14</sup>. For these materials the large spin-orbit interaction leads to a sizeable bond directional spin exchange, whereas the symmetric Heisenberg exchange cancels out by virtue of the edge-sharing octahedra geometry, making them promising candidates for Kitaev physics<sup>12-14</sup>. Still, the remaining Heisenberg interaction,

present due to small structural distortions away from the ideal honeycomb structure,<sup>15</sup> is an adversary to spin liquid formation, and generally favors a spin-ordered ground state<sup>13,16,17</sup>. By modulating spin entropy through finite temperature effects<sup>18,19</sup> or by adding external magnetic fields<sup>20</sup>, one can however stabilize proximate or field-induced spin liquid phases at thermal equilibrium. These spin liquid realizations show emergent behavior expected for the pure Kitaev spin liquid,<sup>10</sup> most notably, fractionalized particle statistics<sup>19</sup> and quantized conduction phenomena.<sup>20</sup>

A case in point is  $\alpha$ -RuCl<sub>3</sub>. This honeycomb Mott insulator has nearly-ideal  $j_{\text{eff}} = \frac{1}{2}$  isospins in highly symmetric octahedra,<sup>21,22</sup> making it possibly the most promising Kitaev spin liquid host studied to date<sup>18-20</sup>. The  $(B, T)$ -plane in Fig. 1 provides the *equilibrium* phase diagram as a function of magnetic field and temperature. Below  $T_N \approx 7$  K, the isospins couple in a zigzag fashion, consistent with the types of magnetic order captured by the Kitaev-Heisenberg model.<sup>13</sup> Strong short-range spin correlations persist between  $T_N$  and the crossover temperature  $T_H \approx 100$  K, hinting at the formation of a proximate spin liquid (pSL) phase within this intermediate temperature regime.<sup>18,23,24</sup> Above 100 K thermal fluctuations bring the system into a conventional paramagnetic phase. An additional tuning parameter is provided by an in-plane magnetic field. A field of  $B_c \approx 7$  T is sufficient to destabilize the zigzag order. For fields between 7-8 T a much-debated field-induced SL is then stabilized,<sup>20</sup> whereas for higher fields a quantum disordered state with partial field alignment of the effective moments forms.<sup>15,25,26</sup>

In this work, we report on the observation of a transient long-lived spin disordered state in the Kitaev-Heisenberg magnet  $\alpha$ -RuCl<sub>3</sub> induced by pulsed light excitation. Holon-doublon pairs are created by photoexcita-

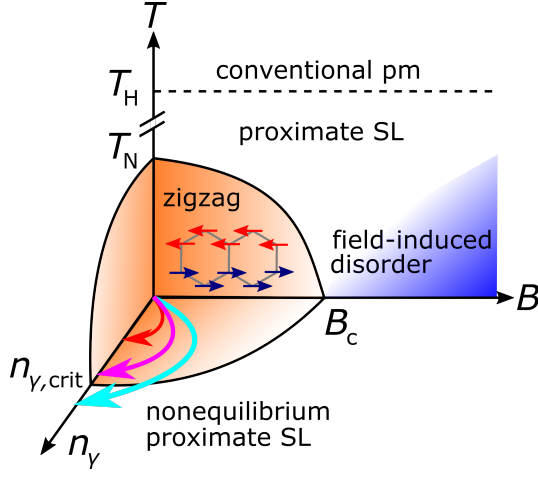


Figure 1. A nonequilibrium dimension to  $\alpha$ -RuCl<sub>3</sub>'s magnetic phase diagram. The  $(B, T)$ -plane sketches the *equilibrium* magnetic phase diagram. Photoexcited holon-doublon pairs  $n_\gamma$  form a new *nonequilibrium* parameter. For small (red) to intermediate (magenta) quenches the system stays inside the zigzag ordered phase. Above a critical density  $n_{\gamma, \text{crit}}$  a nonequilibrium proximate spin liquid state may be induced (light blue arrow).

tion above the Mott gap, and provide a new *nonequilibrium* dimension to  $\alpha$ -RuCl<sub>3</sub>'s magnetic free energy landscape and resulting phase diagram, as illustrated in Fig. 1. The subsequent holon-doublon pair recombination through multimagnon emission leads to a decrease of the zigzag magnetic order. This is tracked through the magnetic linear dichroism (MLD) response of the system. For a sufficiently large holon-doublon density the MLD rotation vanishes, implying that the zigzag ground state is fully suppressed and that a long-lived transient spin-disordered phase is induced. The disordering dynamics of the zigzag order parameter is captured by a time-dependent Ginzburg-Landau model, corroborating the nonequilibrium quasistationary nature of the transient phase. Our work provides insight into the coupling between high-energy electronic and low-energy magnetic degrees of freedom in  $\alpha$ -RuCl<sub>3</sub> and suggests a new route to reach a proximate spin-liquid phase in honeycomb Mott insulators with residual interactions beyond the bond-directional Kitaev exchange.

## RESULTS AND DISCUSSION

The photoinduced change in reflected polarization rotation from  $\alpha$ -RuCl<sub>3</sub> was measured as a function of temperature and photoexcitation density. The sample is excited above the  $\Delta_{\text{MH}} \sim 1.0$  eV Mott-Hubbard gap<sup>27</sup> with a photon energy of  $\hbar\omega \approx 1.55$  eV. The probe light has 2.42 eV photon energy. Under zero-field conditions, two contributions to the total optical polarization rotation  $\theta_{\text{tot}}$  can be distinguished:

$$\theta_{\text{tot}} = \theta_{\text{LD}} + \theta_{\text{MLD}}(\vec{L}^2). \quad (1)$$

The first term  $\theta_{\text{LD}}$ , linear dichroism, originates from the monoclinic distortion of RuCl<sub>3</sub>,<sup>15</sup> and will only show a negligible temperature dependence over the relevant temperature range.<sup>28</sup> The second term  $\theta_{\text{MLD}}$ , magnetic linear dichroism (MLD),<sup>29,30</sup> is proportional to the square of the zigzag antiferromagnetic order parameter  $\vec{L} = \vec{M}_\uparrow - \vec{M}_\downarrow$ , where  $\vec{M}_\uparrow$  and  $\vec{M}_\downarrow$  give the sublattice magnetizations. As such, the MLD rotation provides an optical probe of the zigzag spin order in  $\alpha$ -RuCl<sub>3</sub>.

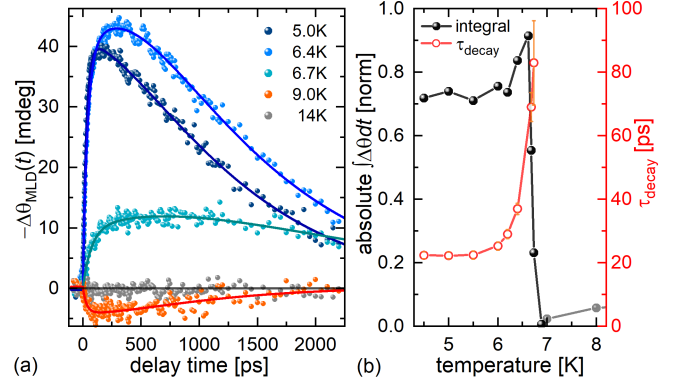


Figure 2. Temperature dependent transient polarization rotation and critical slowing down. a) Photoinduced change in polarization rotation  $-\Delta\theta_{\text{MLD}}(t)$  for various temperatures below and above  $T_N \approx 7$  K. The signal below  $T_N$  is dominated by the proper stacking phase. Above  $T_N$  a small signal with opposite rotational sign is observed, originating from the stacking-fault phase. b) Integrated change in rotation (black spheres) and  $\tau_{\text{decay}}$  [ps] (red circles) as a function of temperature. A critical slowing down of the disordering is observed upon approaching the phase transition.

Figure 2a displays the photoinduced change in polarization rotation  $-\Delta\theta_{\text{MLD}}(t)$  for various bath temperatures. A low-excitation fluence  $F \sim 1.7 \mu\text{J}/\text{cm}^2$  was used, corresponding to a photoexcitation density of  $n_\gamma \approx 0.8 \cdot 10^{17} \text{ cm}^{-3}$  (Ref. 31). For temperatures below  $T_N \approx 7$  K an initial fast demagnetization on the tens of ps timescale is observed, after which the signal recovers on the ns-timescale. Above  $T_N$  a small amplitude response is observed with an opposite rotational sense, originating from a fraction of unavoidable stacking-fault-phase contributions at the sample surface.<sup>27,32</sup> In Fig. 2b the integrated change in rotation  $\Delta\theta_{\text{max}}$  is plotted versus temperature. The integrated rotation change shows a pronounced increase, followed by a rapid reduction upon approaching  $T_N \approx 7$  K. This behavior is qualitatively rationalized by considering that the photoexcitation will have the largest transient effect where the derivative of the zigzag order parameter with respect to temperature is the largest<sup>33</sup>. Concomitantly, we observe a critical slowing down of the disordering upon approaching the phase transition<sup>34,35</sup>. This behavior is well captured by

a  $\tau_{\text{decay}} \propto |1 - T/T_N|^{-\nu z}$  power law with critical exponent  $\nu z = -2.1$ , compatible with the universality class of the 2D Ising model-A dynamics, applicable to  $\alpha\text{-RuCl}_3$ .<sup>33,34,36</sup>

Figure 3a shows the transient rotation traces  $\theta_{\text{MLD}}(t)$  for various initial photoexcitation densities  $n_\gamma$  (sphere symbols). The photoexcitation dependence of the maximum MLD change,  $\Delta\theta_{\text{MLD,max}}$ , is depicted in Fig. 3b. Qualitatively, two excitation regimes can be distinguished. For lower excitation densities ( $n_\gamma < n_{\gamma,\text{crit}} \approx 3 \cdot 10^{17} \text{ cm}^{-3}$ ), the spin system partially disorders, followed by a subsequent recovery. In this regime the disordering time slows down with increasing photoexcitation density. For the high excitation densities ( $n_\gamma > n_{\gamma,\text{crit}} \approx 3 \cdot 10^{17} \text{ cm}^{-3}$ ) a faster disordering time is observed and the change  $\Delta\theta_{\text{MLD,max}}$  saturates (Fig. 3b), implying that the photoexcited system resides in a  $L=0$  state for multiple 100s of ps. Referring to the magnetic phase diagram (Fig. 1 and Refs. 15,20), this means that for quench strengths above  $n_{\gamma,\text{crit}}$  the zigzag order can be fully suppressed, leaving the system in a spin disordered state. The disordering mechanism and the nature of the long-lived transient state is corroborated below.

The inherently strong charge-spin coupling of Mott insulators leads to an efficient nonlinear demagnetization mechanism upon photoexcitation above the Mott-Hubbard gap.<sup>37,38</sup> In order to illustrate this mechanism, first consider the photoexcitation process corresponding to the lowest  $t_{2g}^5 t_{2g}^5 \rightarrow t_{2g}^4 t_{2g}^6$  hopping-type excitation across the Mott-Hubbard gap, as illustrated by the lower hopping process in Fig. 3c. Within a quasiparticle picture, this intermediate excited state corresponds to a spinless *holon* ( $t_{2g}^4$ ) and *doublon* ( $t_{2g}^6$ ), by which effectively two magnetic moments are removed from the zigzag lattice. The mere *creation* of these quasiparticles at the used low densities of 4–85 ppm photons/ $\text{Ru}^{3+}$ -site however does not suffice to explain the magnitude and timescale of the zigzag disordering.<sup>31</sup> Instead, once created, the dominant decay mechanism of the holon-doublon pairs is *recombination* through multimagnon emission (upper hopping process Fig. 3c).<sup>37</sup> An order of magnitude estimate for the released amount of magnons per decayed *hd*-pair is provided by  $\Delta_{\text{MH}}/W \sim 25$  (Refs. 37), with  $W \approx 4.0 \text{ meV}$  being the bandwidth of the low-energy spin wave branch in the zigzag phase.<sup>39</sup> As such, this quasiparticle recombination provides an efficient electronic demagnetization mechanism.

In order to further delineate the excitation mechanism and resulting magnetization dynamics, we model the time-domain data within a dynamic Ginzburg-Landau (GL) model.<sup>34,36</sup> The holon-doublon density, representing the nonequilibrium dimension in Fig. 1, comes in as a new dynamical variable here. We first consider the modified free energy for the antiferromagnetic order parameter  $L$  and the holon-doublon-pair density  $n$ :

$$\mathcal{F}(n, L) = \frac{a_1}{2}(n - n_{\text{c,eq}})L^2 + \frac{a_2}{4}L^4 + \tilde{\mathcal{F}}(n), \quad (2)$$

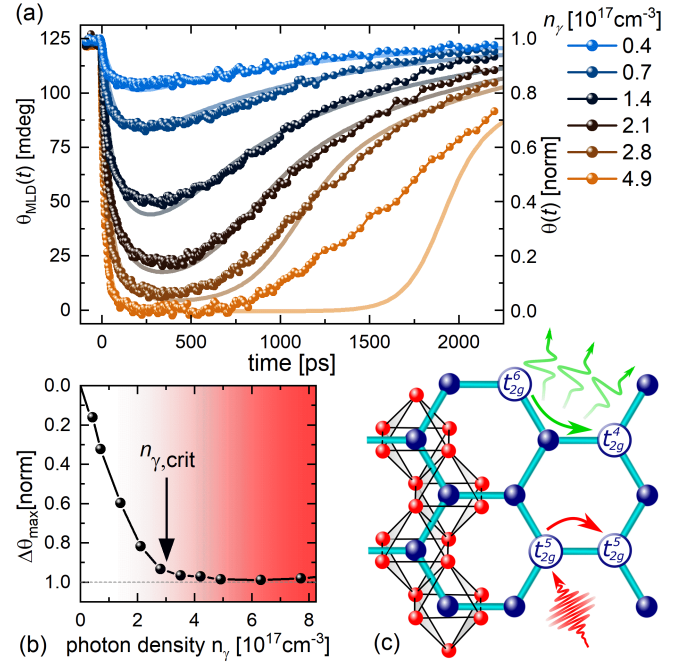


Figure 3. Nonequilibrium magnetic phase transition and holon-doublon pair recombination by multimagnon emission. a) Density-dependent  $\theta_{\text{MLD}}(t)$  for different excitation densities  $n_\gamma$ , as indicated with spheres. The modelled rotation  $\theta(t)$  is indicated with thick lines. b) Maximum change in the magnetic linear dichroism (MLD) rotation  $\Delta\theta_{\text{MLD}}(t)$  as a function of photon density  $n_\gamma$ . Above the critical density  $n_{\gamma,\text{crit}} \approx 3 \cdot 10^{17} \text{ cm}^{-3}$  the maximum change in MLD-rotation saturates. c) The honeycomb lattice, consisting of Ru-sites (dark-blue sites) and chloride ligand ions (red sites). The lower process shows the photogeneration of a holon-doublon pair. The upper process shows the subsequent multimagnon emission by holon-doublon recombination.

with

$$\tilde{\mathcal{F}}(n) = a_3 n + \frac{a_4}{2} n^2 + \frac{a_5}{3} n^3, \quad (3)$$

where  $a_i$ ,  $i = 1, \dots, 5$  are phenomenological parameters. The terms with even powers in the zigzag order parameter  $L$  are the standard symmetry-allowed terms in the Landau free energy expansion for an antiferromagnet.<sup>36,40</sup> Notice that odd powers of  $L$  are ruled out by the inversion symmetry of  $\text{RuCl}_3$ .<sup>15</sup> The initial value of the holon-doublon pair density  $n(0)$ , or quench strength, is taken proportional to the experimental photoexcitation densities  $n_\gamma$ , i.e.,  $n(0) \propto n_\gamma$ , where each photon creates one *hd*-pair. The first term in  $\mathcal{F}(n, L)$ , coupling the *hd*-pair density  $n$  to the order parameter  $L$ , leads to a destabilization of the magnetic order for a sufficiently strong excitation of *hd*-pairs, thus reproducing the process of annihilation of *hd*-pairs into magnons.<sup>37,41</sup> The parameter  $n_{\text{c,eq}}$  is introduced as the critical *hd*-pair density at equilibrium. The functional  $\tilde{\mathcal{F}}(n)$ , independent of the order parameter  $L$ , describes the excess energy of the *hd*-density and its relaxation

in the absence of magnetization. It therefore accounts for decay mechanisms other than the nonradiative multimagnon emission discussed above, such as nonradiative phonon emission, spontaneous decay under radiative emission,<sup>42</sup> and possible  $hd$ -pair diffusion out of the probe volume. The form of  $\tilde{\mathcal{F}}(n)$  is chosen as a third-order polynomial, although its exact form is not crucial for the analysis.

The time evolution of the  $hd$ -pair density  $n$  and magnetic order parameter  $L$  is described by the coupled equations of motion:

$$\frac{dL}{dt} = -\frac{\delta\mathcal{F}}{\delta L}, \quad \frac{dn}{dt} = -\frac{\delta\mathcal{F}}{\delta n}. \quad (4)$$

In order to relate Eqs. (4) to the experimentally measured rotation  $\theta_{\text{MLD}}$ , we rewrite the equations in terms of the polarization rotation  $\theta = L^2/2$ , to finally obtain:

$$\frac{d\theta}{dt} = -2a_1(n - n_{\text{c,eq}})\theta - 4a_2\theta^2, \quad (5a)$$

$$\frac{dn}{dt} = -a_1\theta - \frac{\delta}{\delta n}\tilde{\mathcal{F}}(n) \quad (5b)$$

By using Eq. (5a), the trajectories  $n(t), \theta(t)$  can be modelled for different initial quench strengths  $n(0)$ , taken proportional to the experimental  $n_\gamma$  densities. The curves for  $\theta(t)$  are superimposed on the experimental  $\theta_{\text{MLD}}(t)$  in Fig. 3a. The model captures the dependence of the demagnetization time on the excitation density and the position of  $t_{\text{max}}$ , i.e., the time at which  $\Delta\theta_{\text{max}}$  is reached. For the higher excitation densities the magnetic order vanishes, reproducing the long-lived transient  $L=0$  state. The inclusion of the  $n^3$ -term in  $\tilde{\mathcal{F}}(n)$  ensures that the GL-description does not overestimate the lifetime of the  $L=0$  state.<sup>43</sup> The density-dependent rotation transients are well captured considering the minimal amount of parameters needed in the nonequilibrium GL-description.

The  $hd$ -pair density-dependent free-energy landscape  $\mathcal{F}(n, L)$  is shown in Fig. 4. For low densities, the free energy retains its double-well profile, whereas for higher densities a single well forms.<sup>35</sup> Representative trajectories  $n(t), L(t)$  for different excitation densities are drawn into the free-energy landscape, with colors corresponding to the conceptual trajectories of Fig. 1. The quench  $n(0)$  brings the system into a high-energy state, after which  $n$  and  $L$  relax along the minimal energy trajectory. For a small quench (red trajectory) the zigzag order parameter  $L(t)$  stays finite and eventually recovers. For the intermediate densities (magenta trajectory) the  $n(t), L(t)$  coordinates approach the  $L=0$  line. For the higher excitation densities (light blue trajectory) the  $hd$ -pairs have sufficient excess energy to let  $n(t), L(t)$  follow a trajectory along the  $L=0$  line, i.e., full spin disordering is reached. We emphasize that, for strong quenches, the excitation density  $n(t)$  still varies in time, even though  $L(t)$  takes the quasistationary value  $L(t)=0$ . A sufficiently strong photoexcitation quench thus provides a mechanism to dynamically stabilize a *nonequilibrium quasistationary* spin disordered state in  $\alpha$ -RuCl<sub>3</sub>.

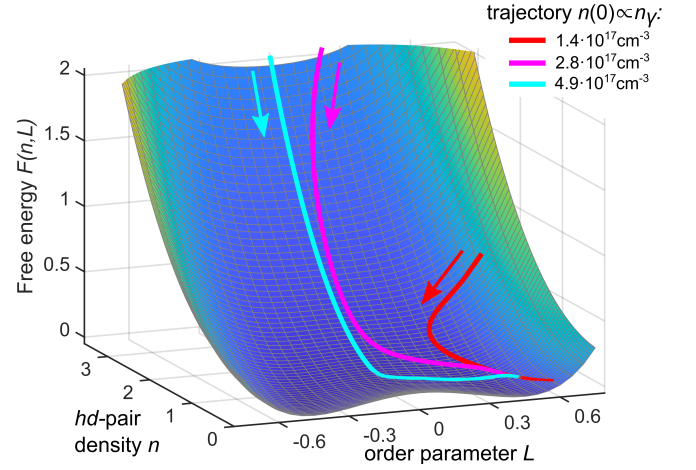


Figure 4. Free energy landscape and nonequilibrium quasistationary spin disordered state. Free energy landscape  $F(n, L)$  as a function of the zigzag order parameter  $L$  and  $hd$ -pair density  $n$  (cf. the phase diagram in Fig. 1). The initial quench  $n(0)$  brings the system to a high energy state, after which the system relaxes. For small quenches (red trajectory), the order parameter  $L$  stays finite under the relaxation of the density  $n$ . For intermediate quenches (magenta trajectory) the system approaches the  $L=0$  line. For strong quenches (light blue trajectory, highest energies not shown) the system relaxes along the  $L=0$  line, implying that the system is described as a nonequilibrium quasistationary spin disordered state.

The maximum lifetime of the nonequilibrium quasistationary spin disordered state is dictated by the recombination rate of the  $hd$ -pairs. The time evolution of  $n(t)$  obtained from the nonequilibrium GL model provides us with an estimate of a few nanoseconds for the recombination timescale of the  $hd$ -pairs.<sup>43</sup> This timescale is expected to grow exponentially with the number of magnons needed to traverse the Mott gap, i.e.,  $\tau \sim e^{\Delta_{\text{MH}}/W}$ .<sup>37</sup> Considering the weak exchange-interaction scale  $W$  in  $\alpha$ -RuCl<sub>3</sub>, one may indeed expect significantly longer recombination times compared to materials with an order of magnitude stronger exchange, such as Nd<sub>2</sub>CuO<sub>4</sub> and Sr<sub>2</sub>IrO<sub>4</sub>, where  $hd$ -pair lifetimes on the order of 0.1 ps have been reported.<sup>38,44</sup> A large ratio between the Mott gap and the exchange interaction energy thus is the key element to ensure a long lifetime of the nonequilibrium quasistationary state.

The microscopic nature of the transient long-lived spin disordered state currently remains elusive. The used low excitation densities by far do not provide sufficient energy to drive the material into a conventional paramagnetic state, nor to change the dominant interactions in the system. Considering the phase diagram, it therefore seems plausible that the system is driven into a transient proximate spin liquid phase, reminiscent of the thermodynamic state just above  $T_N$ . Energy-resolved ultrafast techniques may provide more insight into the microscopic properties of the induced phase.<sup>17,19,45</sup> Further-

more, exact diagonalization<sup>46</sup> and nonequilibrium dynamical mean-field theory<sup>47</sup> methods may elucidate the role of *hd*-excitations in the Kitaev-Heisenberg model and the resulting phase diagram.

## CONCLUSIONS

We have unveiled a pulsed light excitation driven mechanism allowing to trap a Kitaev-Heisenberg magnet into a quasistationary spin disordered state. Photoexcitation above the Mott-gap generates a transient density of holon-doublon quasiparticle pairs. The subsequent recombination of these quasiparticles through efficient multimagnon emission provides a way to dynamically destabilize the competing zigzag ordered ground state and thereby keeps the system in an out-of-equilibrium spin disordered state, up until the transient electronic quasiparticle density gets depleted. Our work provides insight into the coupling between electronic and magnetic degrees of freedom in  $\alpha$ -RuCl<sub>3</sub>, and suggest a new way to reach a proximate spin liquid phase in Kitaev-Heisenberg magnets.

## MATERIALS AND METHODS

*Sample growth and characterization* High-quality  $\alpha$ -RuCl<sub>3</sub> crystals were prepared by vacuum sublimation.<sup>26</sup> Different samples of the batch were characterized by SQUID magnetometry, showing a sharp phase transition at  $T_N \approx 7$ K. This bulk technique can only provide a first indication of sample quality for an optics study. Cleaving or polishing of RuCl<sub>3</sub> samples introduces strain, which

leads to stacking faults. For the optics study, we therefore refrained from any sample treatment, and used an as-grown RuCl<sub>3</sub> sample with a shiny  $\sim 1.5 \times 1.5$  mm<sup>2</sup> surface area. The temperature dependence shown in Fig. 2b shows a clear phase transition at  $T_N \approx 7$ K.

*Time-resolved magneto-optical experiment* The  $\alpha$ -RuCl<sub>3</sub> sample is mounted in a bath cryostat. The time-resolved magneto-optical experiment was performed using 800 nm pump pulses with a temporal width of 40 fs, and probe pulses of 512 nm with a temporal width of 250 fs. The pump and probe beam were focused down to a radius of  $r_{\text{pump}} \approx 39$   $\mu$ m and  $r_{\text{probe}} \approx 25$   $\mu$ m, respectively. The repetition rate of the amplified laser system was set to  $f = 30$  kHz in order to ensure that the system can relax back to the ground state between consecutive pulses. The change in polarization rotation of the reflected probe pulse is measured via a standard polarization bridge scheme. The optical conductivity reported in Ref. 27 and the structural properties reported in Ref. 15 allows us to calculate the photoexcitation densities, as outlined in more detail in the Supplementary Material.<sup>31</sup>

## ACKNOWLEDGEMENTS

The authors thank A. Rosch (Cologne, DE) and Z. Lenarčič (Berkeley, USA) for fruitful discussions. This project was partially financed by the Deutsche Forschungsgemeinschaft (DFG) through Project No. 277146847 - Collaborative Research Center 1238: Control and Dynamics of Quantum Materials (Subprojects No. B05 and No. C04) and through project INST 216/783-1 FUGG. S.D. acknowledges support by the European Research Council (ERC) under the Horizon 2020 research and innovation program, Grant Agreement No. 647434 (DOQS).

\* Corresponding author: rolf.versteeg@epfl.ch; Current address: Laboratoire de Spectroscopie Ultrarapide and Lausanne Centre for Ultrafast Science (LACUS), ISIC-FSB, École Polytechnique Fédérale de Lausanne, CH-1015 Lausanne, Switzerland.

† Corresponding author: pvl@ph2.uni-koeln.de

<sup>1</sup> D. N. Basov, R. D. Averitt, D. Hsieh, Towards properties on demand in quantum materials, *Nat. Mater.* **16**, 1077-1088 (2017).

<sup>2</sup> D. Fausti, R.I. Tobey, N. Dean, S. Kaiser, A. Dienst, M. C. Hoffmann, S. Pyon, T. Takayama, H. Takagi, A. Cavalleri, Light-induced superconductivity in a stripe-ordered cuprate, *Science* **331**, 189-191 (2011).

<sup>3</sup> T. F. Nova, A. S. Disa, M. Fechner, A. Cavalleri, Metastable ferroelectricity in optically strained SrTiO<sub>3</sub>, *Science* **364**, 1075-1079 (2019).

<sup>4</sup> X. Li, T. Qiu, J. Zhang, E. Baldini, J. Lu, A. M. Rappe, K. A. Nelson, Terahertz field-induced ferroelectricity in quantum paraelectric SrTiO<sub>3</sub>, *Science* **364**, 1079-1082 (2019).

<sup>5</sup> A. Kogar, A. Zong, P. E. Dolgirev, X. Shen, J. Straquadine, Y.-Q. Bie, X. Wang, T. Rohwer, I.-C. Tung, Y. Yang,

R. Li, J. Yang, S. Weathersby, S. Park, M. E. Kozina, E. J. Sie, H. Wen, P. Jarillo-Herrero, I. R. Fisher, X. Wang, N. Gedik, Light-induced charge density wave in LaTe<sub>3</sub>, *Nat. Phys.* **16**, 159-163 (2020).

<sup>6</sup> S. W. Teitelbaum, B. K. Ofori-Okai, Y.-H. Cheng, J. Zhang, F. Jin, W. Wu, R. D. Averitt, K. A. Nelson, Dynamics of a persistent insulator-to-metal transition in strained manganite films, *Phys. Rev. Lett.* **123**, 267201 (2019).

<sup>7</sup> P. E. Dolgirev, M. H. Michael, A. Zong, N. Gedik, E. Demler, Self-similar dynamics of order parameter fluctuations in pump-probe experiments, *Phys. Rev. B* **101**, 174306 (2020).

<sup>8</sup> L. Balents, Spin liquids in frustrated magnets, *Nature* **464**, 199-208 (2010).

<sup>9</sup> J. Knolle, R. Moessner, A field guide to spin liquids, *Annu. Rev. Condens. Matter Phys.* **10**, 451-472 (2019).

<sup>10</sup> A. Kitaev, Anyons in an exactly solved model and beyond, *Ann. Phys.* **321**, 2-111 (2006).

<sup>11</sup> C. Broholm, R. J. Cava, S. A. Kivelson, D. G. Nocera, M. R. Norman, T. Senthil, Quantum spin liquids, *Science* **367** (6475), eaay0668 (2020).



- <sup>12</sup> G. Jackeli, G. Khaliullin, Mott insulators in the strong spin-orbit coupling limit: From Heisenberg to a quantum compass and Kitaev models, *Phys. Rev. Lett.* **102**, 017205 (2009).
- <sup>13</sup> J. Chaloupka, G. Jackeli, G. Khaliullin, Zigzag magnetic order in the iridium oxide  $\text{Na}_2\text{IrO}_3$ , *Phys. Rev. Lett.* **110**, 097204 (2013).
- <sup>14</sup> H. Takagi, T. Takayama, G. Jackeli, G. Khaliullin, S. E. Nagler, Concept and realization of Kitaev quantum spin liquids, *Nat. Rev. Phys.* **1**, 264-280 (2019).
- <sup>15</sup> R. D. Johnson, S. C. Williams, A. A. Haghighirad, J. Singleton, V. Zapf, P. Manuel, I. I. Mazin, Y. Li, H. O. Jeschke, R. Valentí, R. Coldea, Monoclinic crystal structure of  $\alpha - \text{RuCl}_3$  and the zigzag antiferromagnetic ground state, *Phys. Rev. B* **92**, 235119 (2015).
- <sup>16</sup> Z. Alpichshev, F. Mahmood, G. Cao, N. Gedik, Confinement-deconfinement transition as an indication of spin-liquid-type behavior in  $\text{Na}_2\text{IrO}_3$ , *Phys. Rev. Lett.* **114**, 017203 (2015).
- <sup>17</sup> N. Nembrini, S. Peli, F. Banfi, G. Ferrini, Yogesh Singh, P. Gegenwart, R. Comin, K. Foyevtsova, A. Damascelli, A. Avella, C. Giannetti, Tracking local magnetic dynamics via high-energy charge excitations in a relativistic Mott insulator, *Phys. Rev. B* **94**, 201119 (2016).
- <sup>18</sup> S.-H. Do, S.-Y. Park, J. Yoshitake, J. Nasu, Y. Motome, Y. Seung Kwon, D.T. Adroja, D.J. Voneshen, K. Kim, T.-H. Jang, J.-H. Park, K.-Y. Choi, S. Ji, Majorana fermions in the Kitaev quantum spin system  $\alpha\text{-RuCl}_3$ , *Nat. Phys.* **13**, 10791084 (2017).
- <sup>19</sup> L. J. Sandilands, Y. Tian, K. W. Plumb, Y.-J. Kim, K. S. Burch, Scattering continuum and possible fractionalized excitations in  $\alpha\text{-RuCl}_3$ , *Phys. Rev. Lett.* **114**, 147201 (2015).
- <sup>20</sup> Y. Kasahara, T. Ohnishi, Y. Mizukami, O. Tanaka, S. Ma, K. Sugii, N. Kurita, H. Tanaka, J. Nasu, Y. Motome, T. Shibauchi, Y. Matsuda, Majorana quantization and half-integer thermal quantum hall effect in a Kitaev spin liquid, *Nature* **559**, 227-231 (2018).
- <sup>21</sup> K. W. Plumb, J. P. Clancy, L. J. Sandilands, V. Vijay Shankar, Y. F. Hu, K. S. Burch, H.-Y. Kee, Y.-J. Kim,  $\alpha - \text{RuCl}_3$ : A spin-orbit assisted Mott insulator on a honeycomb lattice, *Phys. Rev. B* **90**, 041112 (2014).
- <sup>22</sup> S. Agrestini, C.-Y. Kuo, K.-T. Ko, Z. Hu, D. Kasinathan, H. B. Vasili, J. Herrero-Martin, S. M. Valvidares, E. Pellegrin, L.-Y. Jang, A. Henschel, M. Schmidt, A. Tanaka, L. H. Tjeng, Electronically highly cubic conditions for Ru in  $\alpha\text{-RuCl}_3$ , *Phys. Rev. B* **96**, 161107 (2017).
- <sup>23</sup> A. Banerjee, C. A. Bridges, J.-Q. Yan, A. A. Aczel, L. Li, M. B. Stone, G. E. Granroth, M. D. Lumsden, Y. Yiu, J. Knolle, S. Bhattacharjee, D. L. Kovrizhin, R. Moessner, D. A. Tennant, D. G. Mandrus, S. E. Nagler, Proximate Kitaev quantum spin liquid behaviour in a honeycomb magnet, *Nat. Mater.* **15**, 733-740 (2016).
- <sup>24</sup> S. M. Winter, K. Riedl, D. Kaib, R. Coldea, R. Valentí, Probing  $\alpha - \text{RuCl}_3$  beyond magnetic order: Effects of temperature and magnetic field, *Phys. Rev. Lett.* **120**, 077203 (2018).
- <sup>25</sup> J. A. Sears, Y. Zhao, Z. Xu, J. W. Lynn, Y.-J. Kim, Phase diagram of  $\alpha\text{-RuCl}_3$  in an in-plane magnetic field, *Phys. Rev. B* **95**, 180411 (2017).
- <sup>26</sup> A. Sahasrabudhe, D. A. S. Kaib, S. Reschke, R. German, T. C. Koethe, J. Buhot, D. Kamenskyi, C. Hickey, P. Becker, V. Tsurkan, A. Loidl, S. H. Do, K. Y. Choi, M. Grüninger, S. M. Winter, Zhe Wang, R. Valentí, P. H. M. van Loosdrecht. High-field quantum disordered state in  $\alpha - \text{RuCl}_3$ : Spin flips, bound states, and multiparticle continuum, *Phys. Rev. B* **101**, 140410 (2020).
- <sup>27</sup> L. J. Sandilands, C. H. Sohn, H. J. Park, S. Yeun Kim, K. W. Kim, J. A. Sears, Y.-J. Kim, T. Won Noh, Optical probe of Heisenberg-Kitaev magnetism in  $\alpha\text{-RuCl}_3$ , *Phys. Rev. B* **94**, 195156 (2016).
- <sup>28</sup> A. Glamazda, P. Lemmens, S.-H. Do, Y. S. Kwon, and K.-Y. Choi, Relation between Kitaev magnetism and structure in  $\alpha - \text{RuCl}_3$ , *Phys. Rev. B* **95**, 174429 (2017).
- <sup>29</sup> G. A. Smolenskii, R. V. Pisarev, I. G. Sinii, Birefringence of light in magnetically ordered crystals, *Sov. Phys. Usp.* **18** 410-429 (1975). *Sov. Phys. Usp.* **18**, 410429 (1975).
- <sup>30</sup> R. V. Pisarev, B. B. Krichevskov, V. V. Pavlov, Optical study of the antiferromagnetic-paramagnetic phase transition in chromium oxide  $\text{Cr}_2\text{O}_3$ , *Phase Transitions* **37**, 63-72 (1991).
- <sup>31</sup> See the Supplementary Materials (found under the Ancillary files for the Arxiv submission) for the determination of the photoexcited holon-doublon pair density.
- <sup>32</sup> H. B. Cao, A. Banerjee, J.-Q. Yan, C. A. Bridges, M. D. Lumsden, D. G. Mandrus, D. A. Tennant, B. C. Chakoumakos, S. E. Nagler, Low-temperature crystal and magnetic structure of  $\alpha - \text{RuCl}_3$ , *Phys. Rev. B* **93**, 134423 (2016).
- <sup>33</sup> A. Banerjee, J. Yan, J. Knolle, C. A. Bridges, M. B. Stone, M. D. Lumsden, D. G. Mandrus, D. A. Tennant, R. Moessner, S. E. Nagler, Neutron scattering in the proximate quantum spin liquid  $\alpha\text{-RuCl}_3$ , *Science* **356**, 1055-1059 (2017).
- <sup>34</sup> P. C. Hohenberg, B. I. Halperin, Theory of dynamic critical phenomena, *Rev. Mod. Phys.* **49**, 435-479 (1977).
- <sup>35</sup> A. Zong, P. E. Dolgirev, A. Kogar, E. Ergeçen, M. B. Yilmaz, Y.-Q. Bie, T. Rohwer, I.-C. Tung, J. Straquadine, X. Wang, Y. Yang, X. Shen, R. Li, J. Yang, S. Park, M. C. Hoffmann, B. K. Ofori-Okai, M. E. Kozina, H. Wen, X. Wang, I. R. Fisher, P. Jarillo-Herrero, N. Gedik, Dynamical slowing-down in an ultrafast photoinduced phase transition, *Phys. Rev. Lett.* **123**, 097601 (2019).
- <sup>36</sup> U. C. Täuber, *Critical dynamics: a field theory approach to equilibrium and non-equilibrium scaling behavior*, (Cambridge University Press, 2014).
- <sup>37</sup> Z. Lenarčič, P. Prelovšek, Ultrafast charge recombination in a photoexcited Mott-Hubbard insulator, *Phys. Rev. Lett.* **111**, 016401 (2013).
- <sup>38</sup> D. Afanasiev, A. Gatilova, D. J. Groenendijk, B. A. Ivanov, M. Gibert, S. Gariglio, J. Mentink, J. Li, N. Dasari, M. Eckstein, Th. Rasing, A. D. Caviglia, A. V. Kimel, Ultrafast spin dynamics in photodoped spin-orbit Mott insulator  $\text{Sr}_2\text{IrO}_4$ , *Phys. Rev. X* **9**, 021020 (2019).
- <sup>39</sup> A. Banerjee, P. Lampen-Kelley, J. Knolle, C. Balz, A. A. Aczel, B. Winn, Y. Liu, D. Pajerowski, J. Yan, C. A. Bridges, A. T. Savici, B. C. Chakoumakos, M. D. Lumsden, D. A. Tennant, R. Moessner, D.G. Mandrus, S. E. Nagler, Excitations in the field-induced quantum spin liquid state of  $\alpha\text{-RuCl}_3$ , *npj Quantum Mater.* **3**, 8 (2018).
- <sup>40</sup> D. I. Khomskii, *Basic aspects of the quantum theory of solids: order and elementary excitations*, (Cambridge University Press, 2010).
- <sup>41</sup> See the Supplementary Materials (found under the Ancillary files for the Arxiv submission) for the derivation of the relation between the  $H_3$  Hamiltonian from Ref. 37, giving the microscopic interaction mechanism for holon-doublon decay into spin waves, and the Ginzburg-Landau

- term  $\propto nL^2$ .
- <sup>42</sup> M. Mitrano, G. Cotugno, S. R. Clark, R. Singla, S. Kaiser, J. Stähler, R. Beyer, M. Dressel, L. Baldassarre, D. Nicoletti, A. Perucchi, T. Hasegawa, H. Okamoto, D. Jaksch, A. Cavalleri, Pressure-dependent relaxation in the photoexcited Mott insulator ET – F<sub>2</sub>TCNQ: Influence of hopping and correlations on quasiparticle recombination rates, *Phys. Rev. Lett.* **112**, 117801 (2014).
- <sup>43</sup> See the Supplementary Materials (found under the Ancillary files for the Arxiv submission) for details of the nonequilibrium Ginzburg-Landau model.
- <sup>44</sup> H. Okamoto, T. Miyagoe, K. Kobayashi, H. Uemura, H. Nishioka, H. Matsuzaki, A. Sawa, and Y. Tokura, Photoinduced transition from Mott insulator to metal in the undoped cuprates Nd<sub>2</sub>CuO<sub>4</sub> and La<sub>2</sub>CuO<sub>4</sub>, *Phys. Rev. B* **83**, 125102 (2011).
- <sup>45</sup> G. B. Halász, N. B. Perkins, J. van den Brink, Resonant inelastic x-ray scattering response of the Kitaev honeycomb model, *Phys. Rev. Lett.* **117**, 127203 (2016).
- <sup>46</sup> Satoshi Okamoto, Global phase diagram of a doped Kitaev-Heisenberg model, *Phys. Rev. B* **87**, 064508 (2013).
- <sup>47</sup> H. Aoki, N. Tsuji, M. Eckstein, M. Kollar, T. Oka, P. Werner, Nonequilibrium dynamical mean-field theory and its applications, *Rev. Mod. Phys.* **86**, 779-837 (2014).